DOI: 10.1002/ejic.201000487

From Salicylaldehyde to Chiral Salen Sulfonates – Syntheses, Structures and Properties of New Transition Metal Complexes Derived from Sulfonato Salen Ligands

Émilie Delahaye,[a] Mayoro Diop,[a] Richard Welter,[b] Mauro Boero,[a,c] Carlo Massobrio,[a] Pierre Rabu,*[a] and Guillaume Rogez*[a]

Keywords: Salen sulfonates / Chirality / Structure elucidation / Ferromagnetic coupling / Density functional calculations

Coordination complexes derived from chiral and nonchiral sulfonato salen ligands {($SalenSO_3$)Na_2: *N*,*N*′-bis(5-sulfonatosalicylidene)-1,2-diaminoethane disodium salt, [(*R*,*R*) and (*S*,*S*)-$CySalenSO_3$]NaK: (*R*,*R*) and (*S*,*S*)-*N*,*N*′-bis(5-sulfonatosalicylidene)-1,2-diaminocyclohexane sodium–potassium salt} have been synthesized. The crystal structures of the chiral and nonchiral Ni^{II} complexes [Ni($SalenSO_3$)]Na_2 (**1**) and [Ni((*R*,*R*)$CySalenSO_3$)]NaK (**2**) were solved. The other chiral and nonchiral sulfonato salen complexes, [Cu($SalenSO_3$)]Na_2 (**4**), [Cu((*R*,*R*)$CySalenSO_3$)]NaK (**5**), [Cu((*S*,*S*)$CySalenSO_3$)]NaK (**6**) and [Zn($SalenSO_3$)]Na_2 (**7**) got hydrolyzed before suitable crystals could form. Yet, their hydrolysis led to the formation of single crystals of the residues of total or partial hydrolysis: 5-sulfonatosalicylaldehyde sodium salt (**A**), *N*-(5-sulfonatosalicylidene)-1,2-diaminoethane copper(II) [Cu($SalSO_3$)] (**8**) and (*R*,*R*)-*N*-(5-sulfonatosalicylidene)-1,2-diaminocyclohexane copper(II) {Cu[(*R*,*R*)$CySalSO_3$]} (**9**). All compounds were studied with IR and UV/Vis spectroscopy; chiral compounds were also investigated by circular dichroism. The magnetic properties of the copper compounds were investigated. Whereas **8** shows intermolecular antiferromagnetic interactions between mononuclear Cu^{II} complexes, **7** presents a weak intramolecular ferromagnetic coupling (J = 0.66 cm^{-1}, $H = -J\hat{\mathbf{S}}_{\mathbf{Cu1}}\hat{\mathbf{S}}_{\mathbf{Cu2}}$), which has been rationalized by DFT calculations.

Introduction

Complexes derived from *N*,*N*′-bis(salicylidene)1,2-diaminoethane or salen present a great interest in catalysis, possibly enantioselective when chiral salen-type complexes are used.[1–4] Salen-type complexes have been used in many reactions like alkene epoxidation,[5,6] epoxide ring opening,[7] cyclopropanations,[8] aziridination[9] and other reactions.[10–12] They can also serve as metalloprotein models, as these complexes are efficient oxygen carriers.[13] Finally, their properties of luminescence can be exploited.[14] One of the main advantages of this family of complexes, generally accessible in high yields, is that they are very versatile.[15,16] It is actually relatively easy to change the substitution of the phenolate groups (by synthesizing the corresponding salicylaldehyde) or to play with the nature of the central bridge.[17–19] In that way, steric hindrance or electronic properties, for instance, can be modified almost at will.

To develop a "green" chemistry and to solve the problem of the recovery of salen-type complexes when used as homogeneous catalysts, many efforts have been made to develop heterogeneous catalysts. They have been entrapped in porous hosts (zeolites) via the "ship in a bottle" approach,[20–23] covalently linked to a support,[24–26] or inserted into porous or lamellar compounds via electrostatic interactions.[27–29] In the case of cationic matrixes such as layered double hydroxides (LDHs), in which the insertion proceeds via an anionic exchange, or in order to build metal organic frameworks (MOFs), it is necessary to functionalize the salen ligands by anchoring groups (carboxylates[30–32] or sulfonates[33,34]). In particular, trivalent metal salen complexes bearing sulfonato groups (with M = Mn^{3+}, Fe^{3+} and Co^{3+}) were inserted into LDHs.[35–38] However, although numerous crystal structures of salen-type complexes were reported in the literature, very few examples are known for salen ligands functionalized with sulfonate groups.[39]

Actually, very few sulfonato-salen-type complexes have been described, mostly with M^{III} ions (M = Mn, Fe and Co),[35–38] with V (IV and V)[40] or recently with Mo^{VI}.[39] In this paper, we describe the synthesis and characterization of nonchiral and chiral sulfonato-salen Ni^{II}, Cu^{II} and Zn^{II} complexes (Scheme 1): [Ni($SalenSO_3$)]Na_2 (**1**) (the synthesis of which has been described previously[41]), [Ni((*R*,*R*)$CySa$-

[a] IPCMS, UMR CNRS-UdS 7504, 23 rue du Loess, B. P. 43, 67034 Strasbourg cedex 2, France
Fax: +33-3-88107247
E-mail: rabu@ipcms.u-strasbg.fr
rogez@ipcms.u-strasbg.fr
[b] Laboratoire Decomet, Institut de Chimie de Strasbourg (UMR CNRS-UdS 7177), 4 rue Blaise Pascal, 67000 Strasbourg, France
[c] Research Center for Integrated Science, Japan Advanced Institute of Science and Technology (JAIST), Hokuriku University, Japan

Supporting information for this article is available on the WWW under http://dx.doi.org/10.1002/ejic.201000487.

lenSO$_3$)]NaK (**2**), [Ni((*S*,*S*)CySalenSO$_3$)]NaK (**3**), [Cu(SalenSO$_3$)]Na$_2$ (**4**), [Cu((*R*,*R*)CySalenSO$_3$)]NaK (**5**), [Cu((*S*,*S*)CySalenSO$_3$)]NaK (**6**) and [Zn(SalenSO$_3$)]Na$_2$ (**7**) {SalenSO$_3^{2-}$ = *N*,*N*′-bis(5-sulfonatosalicylidene)-1,2-diaminoethane and CySalenSO$_3^{2-}$ = *N*,*N*′-bis(5-sulfonatosalicylidene)-1,2-diaminocyclohexane}. All complexes have been characterized by IR and UV/Vis spectroscopy; chiral complexes were also investigated by circular dichroism.

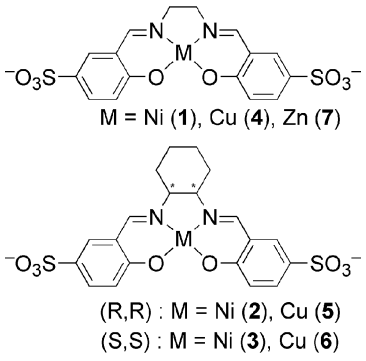

Scheme 1. Schiff base complexes presented in this work: *N*,*N*′-bis(5-sulfonatosalicylidene)-1,2-diaminoethane metal(II) [M(SalenSO$_3$)]$^{2-}$ (top) {M = Ni^{II} (**1**), Cu^{II} (**4**), Zn^{II} (**7**)} and (*R*,*R*) or (*S*,*S*)-*N*,*N*′-bis(5-sulfonatosalicylidene)-1,2-diaminocyclohexane metal(II) [M((*R*,*R*)or(*S*,*S*)CySalenSO$_3$)]$^{2-}$ (bottom) {(*R*,*R*): M = Ni^{II} (**2**), Cu^{II} (**5**); (*S*,*S*): M = Ni^{II} (**3**), Cu^{II} (**6**)}.

The obtained complexes are very soluble in water, due to the presence of the sulfonate groups. The instability of the imine bond with respect to hydrolysis, which depends on the nature of the coordinated metal, prevented the formation of crystals suitable for X-ray diffraction for Cu^{II} and Zn^{II} complexes, but it has been possible to isolate compounds corresponding to different stages of the ligand hydrolysis and to solve their crystal structures (Scheme 2). Ni^{II} analogues were obtained, and the crystal structures of [Ni(SalenSO$_3$)]Na$_2$ (**1**) and [Ni((*R*,*R*)CySalenSO$_3$)]NaK (**2**) were solved. In addition, [Cu(SalSO$_3$)] (**8**) and [Cu((*R*,*R*)-CySalSO$_3$)] (**9**) {SalSO$_3^-$ = *N*-(5-sulfonatosalicylidene)-1,2-diaminoethane, (*R*,*R*)CySalSO$_3^-$ = (*R*,*R*)-*N*-(5-sulfonatosalicylidene)-1,2-diaminocyclohexane} were isolated from the hydrolysis of the Cu^{II} complexes **4** and **5**. Their magnetic properties are discussed.

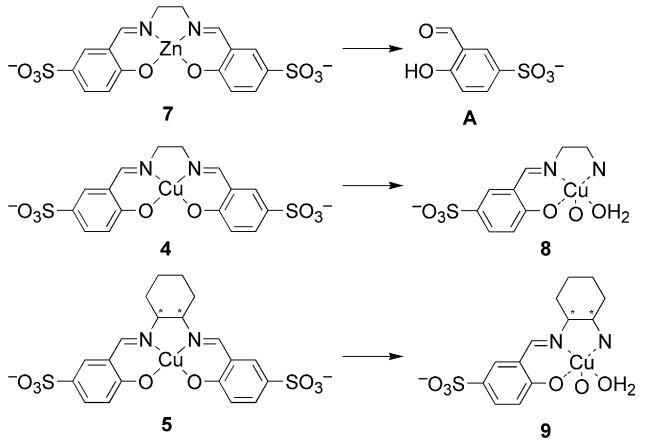

Scheme 2. Hydrolysis of some of the salen-type complexes during the crystallization process.

Results and Discussion

The synthesis of the SalenSO$_3$ and CySalenSO$_3$ complexes has been achieved by using two different procedures, depending on the ligand and on the metal. To synthesize Ni(SalenSO$_3$)Na$_2$ (**1**) and Zn(SalenSO$_3$)Na$_2$ (**7**), it was necessary to obtain first the intermediate di-5-sulfonatosalicylaldehyde metal complex and then to carry on with the formation of the desired complex using a template synthesis.[42] The other method, used to obtain [Ni((*R*,*R*)CySalenSO$_3$)]-NaK (**2**), [Ni((*S*,*S*)CySalenSO$_3$)]NaK (**3**), [Cu(SalenSO$_3$)]-Na$_2$ (**4**), [Cu((*R*,*R*)CySalenSO$_3$)]NaK (**5**) and [Cu((*S*,*S*)CySalenSO$_3$)]NaK (**6**), is more classical, involving the complete synthesis of the ligand before complexation. The first method is likely to provide much more versatility in the sense that it allows to vary the nature of the central diamino bridge rather easily, yet, despite many attempts we did not manage to use it for the synthesis of complexes other than **1** and **7**.

Crystal Growth and Description of the Structures

The main difficulty in obtaining crystals of the complexes above lies in their rather small stability towards hydrolysis. It is well known that imines are unstable in water but much more stable when coordinated to a transition metal ion.[4] Nevertheless, in the present case, the presence of the sulfonate groups apparently counteracts this stabilization. In addition, due to these groups, the complexes are only soluble in water (and in dimethyl sulfoxide). Therefore, the choice of solvents to perform crystallization was really limited, and during the very long times necessary to obtain crystals, hydrolysis is likely to occur.

Various attempts to grow crystals were carried out. The best results were obtained by slow evaporation of a solvent/antisolvent (water/ethanol) mixture, or by slow diffusion (in the liquid phase) of the antisolvent (2-propanol) in an aqueous solution of the aimed compound. Yet the crystallization times remained very long (several weeks to several months), and hydrolysis could not always be avoided. It is worth noting that another approach consisting of mixing very slowly the two reactants (ligand and metal salt, or diamino bridge and di-5-sulfonatosalicylaldehyde intermediate complex) in order to synthesize the desired complexes and grow crystals simultaneously was inefficient here.

Every attempt to obtain crystals of [Zn(SalenSO$_3$)]Na$_2$ (**7**) led to the full hydrolysis of the complex and of the ligand itself; we finally managed to obtain crystals of the 5-sulfonatosalicylaldehyde sodium salt (C$_7$H$_5$O$_5$SNa) (**A**). The structure of the crystals obtained directly from **A** is identical to that obtained from the hydrolysis of **7**, yet the quality of the crystals was worse when obtained directly from **A**. Compound **A** crystallizes in the space group $P2_1/a$

[a = 6.143(4) Å, b = 22.191(9) Å, c = 6.745(4) Å, β = 98.43(3)°]. It crystallizes along with one water molecule per molecular unit. Its structure consists of a 2D arrangement of the 5-sulfonatosalicylaldehyde sodium salt in the (a,b) plane (Figure 1). Within the (a,b) plane, the 5-sulfonatosalicylaldehyde forms pairs, held together by sodium cations in an octahedral O_6 environment (Figure 2). Each Na^+ cation is linked to one sulfonate group (O6) of one 5-sulfonatosalicylaldehyde and the $O_{aldehyde}$ (O2b) atom of the other member of the dimer. Moreover it is also coordinated to another sulfonate group (O3c) of the following dimer along the a direction. Finally, it is coordinated to another sulfonate group (O2a) of the next dimer along b. The coordination sphere of the Na^+ cation is completed by two water molecules (O5 and O5d). The Na^+ cations, bridged by one μ water molecule, one (κ^1)-μ_2 sulfonate (O2) and one (κ^1-κ^1)-μ_2 sulfonate (O3), therefore form chains along a. Each sulfonate is therefore in the (κ^1)-(κ^1-μ_2)-μ_3 coordination mode. Finally, the noncoordinated oxygen atom of the sulfonate groups (O1) plays a very important role in the cohesion of the structure along the c axis, via hydrogen bonds with the hydrogen atoms of the water molecules of the adjacent layer (O1–H2 and O1–H4) (Table S1).

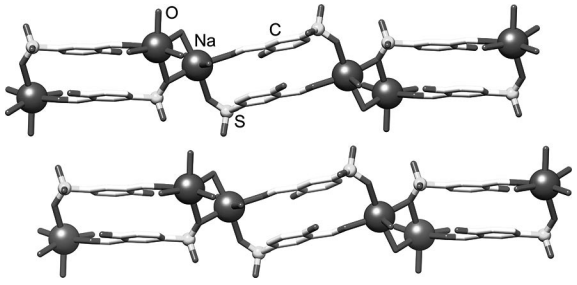

Figure 1. Selected packing view of crystal structure of **A** with partial labelling scheme [(b,c) projection]. Hydrogen atoms have been omitted for clarity.

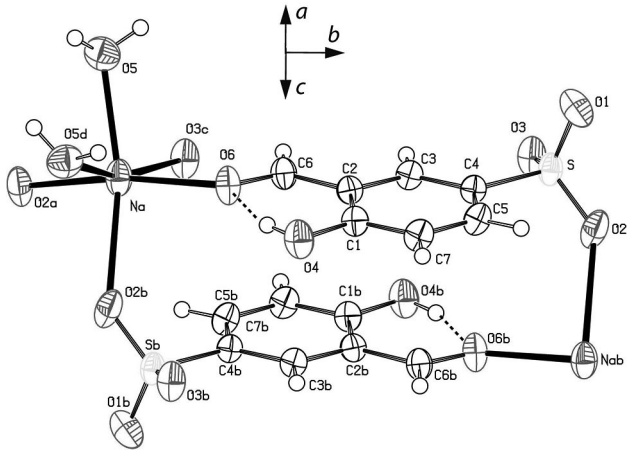

Figure 2. ORTEP view of ligand **A** with full labelling scheme. The ellipsoids enclose 50% of the electronic density. Dashed lines indicate the main intramolecular hydrogen bonds [O4···H1···O6: 0.84(4) Å, 1.88(4) Å, 2.665(4) Å, 156(3)°]. Code for equivalent positions (a): 2.5 – x, –0.5+y, 1 – z; (b): 2 – x, 1 – y, 1 – z; (c): 3 – x, 1 – y, 1 – z; (d): –0.5 + x, 0.5 – y, z.

Attempts for crystallizing copper compounds **4** and **5** lead to only partial hydrolysis of the complexes and to the formation of the new compounds *N*-(5-sulfonatosalicylidene)-1,2-diaminoethane copper(II) (**8**) and (*R*,*R*)-*N*-(5-sulfonatosalicylidene)-1,2-diaminocyclohexane copper(II) (**9**), in which only one imine function has been hydrolyzed. Complex **8** crystallizes in the space group $P2_1/n$ [a = 7.507(5) Å, b = 10.330(5) Å, c = 14.714(8) Å, β = 95.79(3)°]. The asymmetric unit contains two complexes, which result from hydrolysis of one of the two imine groups of the SalenSO$_3$ ligand, the resulting aldehyde fragment being no longer present in the structure. These two complexes are arranged in a head-to-tail fashion, forming a dimer coordinated via the sulfonate groups (Figure 3). This arrangement is similar to the one recently described by Bibal et al. for a Mo^{VI} complex with a sulfonato tridentate Schiff base ligand.[39] Each copper(II) ion is coordinated by the tridentate ligand in *mer* position. The distorted square-pyramidal environment is completed by one O atom coming from a water molecule in the apical position and one O atom coming from the sulfonate group of the other complex of the dimer in the axial position. The five-coordinate geometry around the metal centre can further be described by using the Addison τ parameter, which allows to characterize continuously the geometry between trigonal-bipyramidal (τ = 1) and square-pyramidal (τ = 0) coordination.[43] In the present case, τ = 0.38, which indicates a significant deviation from square-pyramidal geometry. The bond length between the Cu ion and the axial sulfonate oxygen atom is far larger than the other Cu–L distances due to the Jahn–Teller effect [d(Cu–O3) = 2.253 Å, whereas the other Cu–O distances are in the range 1.911–2.017 Å]. As for the structure of the ligand, the C–N distance is around 1.28 Å, which proves that the double bond character has been preserved.

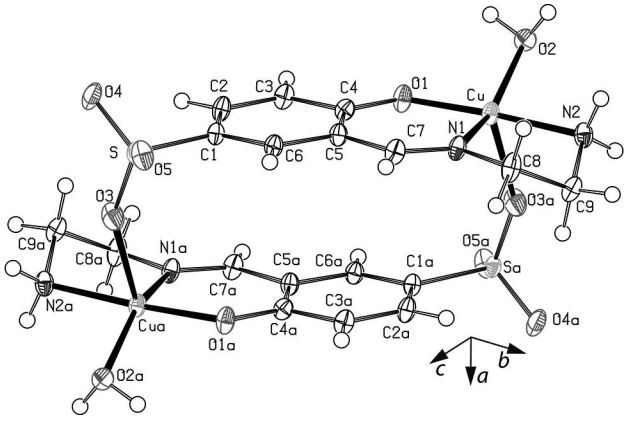

Figure 3. ORTEP view of complex **8** with full labelling scheme. The ellipsoids enclose 50% of the electronic density. Code for equivalent positions: (a): 2 – x, –y,1 – z.

The structure is made of isolated dimers, stacked in columns parallel to the a axis and oriented in herring bones along the (b,c) plane (Figure 4). The complexes are held together within the columns by hydrogen bonds involving the sulfonate group from one side and the terminal amine group and the apical water molecule from the other side

(N2H1–O4 and O2H1–O5) (Table S5). Between the columns, cohesion is also provided by hydrogen bonds involving the sulfonate group and the apical water molecule (O2H2–O4) (Table S4).

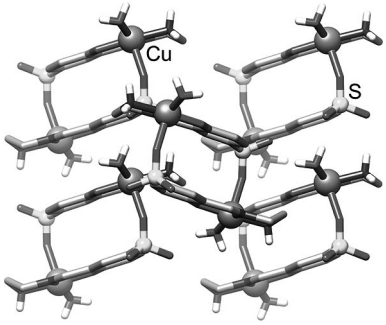

Figure 4. Selected packing view of complex **8** with partial labelling scheme [(*a*,*b*) projection].

Complex **9** crystallizes in the noncentrosymmetric space group $P\bar{1}$ [a = 9.3920(3) Å, b = 9.6840(3) Å, c = 10.7060(3) Å, α = 64.215(2)°, β = 76.243(2)°, γ = 72.652(2)°]. The asymmetric unit contains two complexes. As for the previous case, the complex results from hydrolysis of one of the two imine groups of the ligand, the resulting aldehyde fragment being no longer present in the structure. Each copper(II) ion lies in a slightly distorted square-pyramidal environment (τ = 0.16) made by two N and one O atoms coming from the Schiff base ligand and by two other O atoms from water molecules (Figure 5). The length of the bond between the Cu ion and the axial water oxygen atom is far larger than the other Cu–L distances due to the Jahn–Teller effect [d(Cu1–O3) = 2.297 Å and d(Cu2–O9) = 2.265 Å, whereas the other Cu–O distances are in the range 1.914–2.017 Å]. As in the case of **8**, the C–N distance, around 1.28 Å, is an indication that the double bond character was maintained.

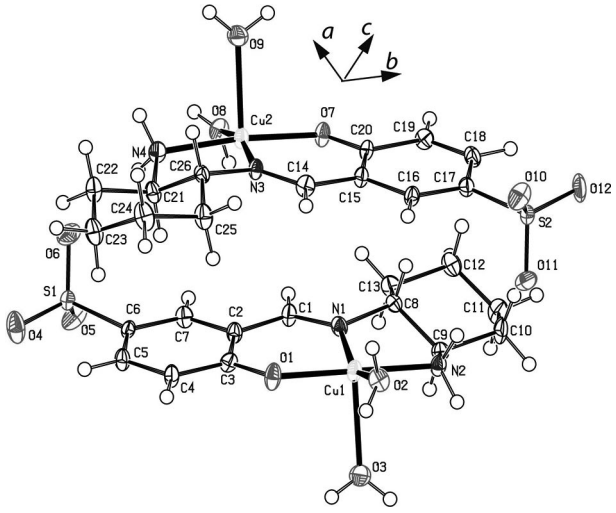

Figure 5. ORTEP view of complex **9** with full labelling scheme. The ellipsoids enclose 50% of the electronic density. H_2O solvent molecules have been omitted for clarity.

The structure is actually made of isolated quasi-planar complexes forming a 2D arrangement (Figure 6). The complexes are held together by two kinds of supramolecular interactions (Table S5): CH–π interactions between C21–H21 and C8–H8 and the centroid of the C2–C7 and C15–C20 aromatic rings, respectively, as well as hydrogen bonds between sulfonate and terminal amine groups (N4H4–O6 and N2H3O11) favouring the head-to-tail organization of the complexes. Hydrogen bonds between sulfonate groups and axially coordinated water molecules provides the 3D cohesion of the molecules (O8H2–O10, O9H1–O4, O9H2–O11, O3H1–O12, O3H2–O6 and O2H2–O5).

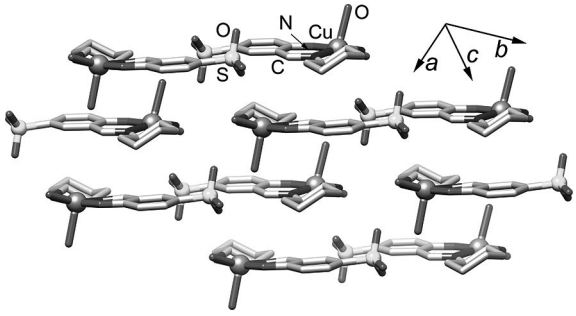

Figure 6. Selected packing view of complex **9** with partial labelling scheme Hydrogen atoms and solvent molecules (H_2O) have been omitted for clarity.

Finally, nickel complexes **1** and **2** crystallized without demetallation or hydrolysis. Crystallization of **1** leads to complex **1′** crystallizing in the space group $P\bar{1}$ [a = 13.3760(10) Å, b = 13.6210(10) Å, c = 15.0400(10) Å, α = 68.16(2)°, β = 80.03(2)°, γ = 82.74(2)°]. The crystal structure shows that the ligand has remained intact and coordinates the Ni^{II} cation in square-planar geometry, as expected for tetradentate salen-type ligands (Figure 7). The imine functions are preserved (the C_{aryl}–N bond length is around 1.296 Å). The complexes are organized in dimers, in which the two nickel complexes are related to each other by an inversion centre. These dimers are organized in planes parallel to the b axis (Figure 8). Within the planes, the dimers are organized in chains held together by a complex arrangement of Na^+ cations (Figures 8 and 9). The Na^+ cations are bridged by water molecules and by the sulfonate groups. Each sulfonate adopts a (κ^1-κ^2-μ_2)-(κ^2-κ^2-μ_2)-(κ^1-κ^2-μ_2)-μ_4 coordination mode (Scheme 3).

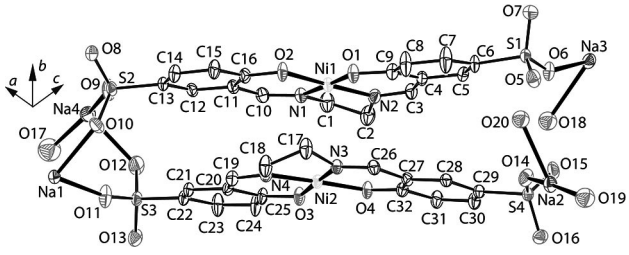

Figure 7. ORTEP view of the asymmetric unit of complex **1′** with full labelling scheme. The ellipsoids enclose 50% of the electronic density. H_2O solvent molecules and hydrogen atoms have been omitted for clarity.

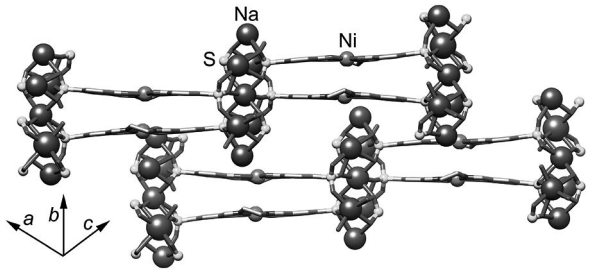

Figure 8. Selected packing view of complex **1′** with partial labelling scheme in (*a*,*b*) projection.

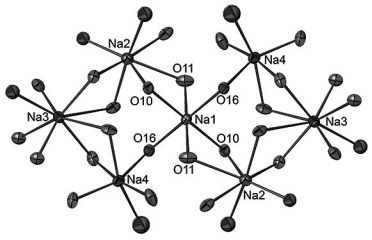

Figure 9. Connection of the different kinds of Na^+ centred polyhedra in the crystal of **1′**.

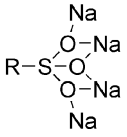

Scheme 3. $(\kappa^1\text{-}\kappa^2\text{-}\mu_2)\text{-}(\kappa^2\text{-}\kappa^2\text{-}\mu_2)\text{-}(\kappa^1\text{-}\kappa^2\text{-}\mu_2)\text{-}\mu_4$ coordination mode of the sulfonate groups in **1′**.

Twenty two water molecules per asymmetric unit have been found in the crystal structure (a squeeze procedure has been used), six of which are coordinated to Na^+ ions (O19 and O20 to Na2 and O17 to Na4). H_2O solvent molecules are located in between the planes and contribute to the stabilization of the edifice via an intricate hydrogen-bond network (Table S2), yet given the quality of the structure, it is not reasonable to go further in the description of their organization. Finally, it is worth noting that compound **1′** obtained from the crystallization of **1** presents from the crystal structure resolution only seven Na^+ ions for eight sulfonate groups, whereas **1** is obtained, as a powder, as a fully deprotonated compound, with two sodium counterions and three molecules of water, as determined from elemental analysis. This situation comes from a special position found for one Na^+ ion placed on the symmetry centre of the $P\bar{1}$ group. Attempts in noncentrosymmetric space group ($P1$) did not give a better solution for this crystal structure. One reasonable hypothesis given the important number of water molecules found in **1′** is that this lack of one positive charge might be compensated by one proton, which unfortunately cannot be located by X-ray diffraction.

Complex **2** crystallizes in the noncentrosymmetric space group $P2_1$ [a = 11.8260(9) Å, b = 6.8820(3) Å, c = 18.5710(13) Å, β = 91.256(3)°], along with five water molecules, three of which are coordinated to sodium cations. As for **1**, the structure confirms that the ligand has remained intact, the C_{aryl}–N bond length ranging between 1.280 and 1.292 Å. Moreover, the homochirality is confirmed by the Flack parameter of 0.05(2). The chiral tetradentate Schiff base ligand coordinates the Ni^{II} cation in square-planar geometry (Figure 10). The complexes adopt a 2D organization, and all complexes are parallel to the (*a*,*c*) plane. The connection between the complex in the (*a*,*c*) plane and along the *b* axis is achieved by Na^+ an K^+ cations. The presence of K^+ cations results from the use of K_2CO_3 during the synthesis of the ligand. Any attempt to replace this base by another one (for instance Na_2CO_3) was unsuccessful. The presence of both Na^+ and K^+ cations is confirmed by the elemental analysis (see Experimental Section). These cations form layers parallel to the (*a*,*b*) plane; they both lie in an octahedral environment, sharing one face (O8–O9–O5) (Figure 11). They are bridged by water molecules and by sulfonate groups. Each sulfonate adopts a $(\kappa^1\text{-}\kappa^2\text{-}\mu_2)\text{-}(\kappa^1\text{-}\kappa^2\text{-}\mu_2)\text{-}\mu_3$ coordination mode with one noncoordinated oxygen atom, which is implied in hydrogen bonds with water molecules bridging Na^+ and K^+ cations and with noncoordinated water molecules present in the structure (Table S3).

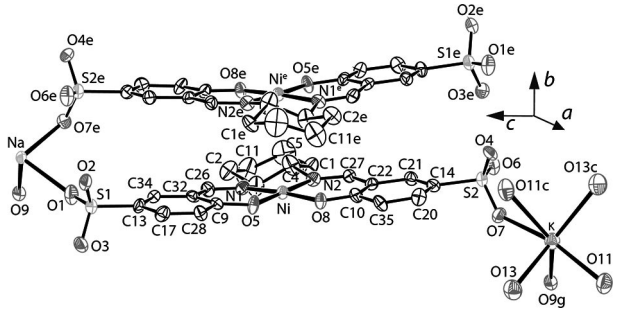

Figure 10. ORTEP view of complex **2** with partial labelling scheme. The ellipsoids enclose 50% of the electronic density. H_2O solvent molecules have been omitted for clarity. Codes for equivalent positions: (e): $2 - x, -1/2 + y, 1 - z$; (c): $1 - x, -1/2 + y, -z$.

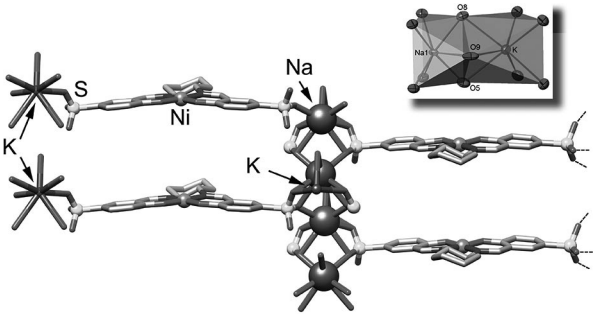

Figure 11. Selected packing view of complex **2** with partial labelling scheme in (*b*,*c*) projection. Hydrogen atoms and H_2O solvent molecules have been omitted for clarity. Short dashed lines show where the polymer has been "cut" for this selected view. The inset shows face-shared polyhedra around Na^+ and K^+.

Full rationalization of the differences observed in hydrolysis rates is rather difficult, because many thermodynamic and kinetic parameters are implied. First, Ni^{II} salen-type complexes are indeed generally more stable (thermodynami-

Table 1. Attribution of some characteristic absorption bands for **A**, **1**, **2**, **4**, **5**, **7**, **8** and **9** (in cm^{-1}).

	$\nu_{NH2asym}$	ν_{NH2sym}	$\nu_{CH2asym}$	ν_{CH2sym}	$\nu_{C-Hald.}$	$\nu_{C=N}$	$\nu_{C=O}$	$\nu_{SO3asym}$	ν_{SO3sym}	$\Delta\nu_{SO3}$
A	–	–	–	–	2897	–	1654	1174	1038	136
1	–	–	sh	sh	–	1611	–	1172	1042	130
2	–	–	2938	2863	–	1624	–	1178	1032	146
4	–	–	2938	2862	–	1641	–	1174	1033	141
5	–	–	2940	2855	–	1635	–	1185	1032	153
7	–	–	2934	2862	–	1641	–	1169	1045	124
8	3240	3155	2920	2858	–	1648	–	1194	1034	160
9	3313	3243	2948	2863	–	1639	–	1190	1034	156

cally) than those with Cu^{II}.[41] Then, another important aspect is the lability of the complex, which leads to partial or full hydrolysis due to instability of the ligand in water when decomplexed. Finally, the pH of the reaction is also a crucial parameter,[41] yet it is somewhat difficult to control during the complexation process and to avoid the formation of metal hydroxide or oxide.

Infrared Spectroscopy

Figures S1, S2 and S3 show the IR spectra of compounds **A**, **1**, **2**, **4**, **5**, **7**, **8** and **9** recorded in KBr pellets. In Table 1 the positions of the main absorption bands discussed below are collected. IR spectra of **3** and **6** are identical to those for **2** and **5** respectively.

The infrared spectra of all the compounds show bands in the 3700–3200 cm^{-1} region, indicative of the presence of water (H_2O stretching bands). These bands may be more or less narrow or structured, depending on the involvement of the water molecules in hydrogen bonds.

For all compounds (except **A**), two weak and rather narrow absorption bands appear in the range 2950–2850 cm^{-1} and can be attributed to the CH_2 asymmetric and symmetric stretching modes.

For **A**, the absorption band at 2897 cm^{-1} can be attributed to the CH stretching of the aldehyde group, while the band at 1654 cm^{-1} is due to C=O stretching.[44] These two bands are absent in the other compounds.

The IR spectra of **7** and **8** show characteristic features due to the partial hydrolysis of the ligand. Actually, two rather narrow absorption bands appear between 3350 and 3200 cm^{-1}, assigned to the asymmetric and symmetric NH_2 stretching modes, respectively.[44]

The imine group gives rise to a band around 1630 cm^{-1}, which is very intense in the case of the compounds bearing the full salen ligands **1**, **2**, **4**, **5** and **7** but much more difficult to identify in copper compounds **7** and **8**, which possess only one imine group. Moreover, for **7** and **8**, this band is superimposed with the band due to the bending of the NH_2 group at 1648 cm^{-1} and 1639 cm^{-1} for **7** and **8**, respectively.

All spectra show intense bands in the 1230–1120 cm^{-1} and 1080–1025 cm^{-1} ranges attributed to antisymmetric $\nu_{as}(SO_3)$ and symmetric $\nu_{sym}(SO_3)$ stretching modes, respectively. Similarly to carboxylate,[45–47] the study of the difference between ν_{as} and ν_{sym} can bring information on the coordination mode of the sulfonate groups.[48,49] Yet, due to the relatively small number of structures of molecules bearing sulfonate groups, correlations between coordination of the sulfonate group and IR spectroscopic features are rather scarce. The examples described in this study show a general tendency. When sulfonato groups are either not coordinated (case of **8**) or monodentately coordinated to a metal (case of **7**), the value of $\Delta\nu$ is much higher (160 and 156 cm^{-1} for **8** and **7**, respectively) than that observed in compounds with sulfonato groups coordinated to two or three Na^+ (146, 136 and 130 cm^{-1} for **2**, **A** and **1**, respectively).

UV/Vis Spectroscopy and Circular Dichroism

Solid-state spectra were recorded with an integrating sphere on pure ground samples for electronic spectra and, in transmission, on ground samples in KBr pellets for CD spectra. UV/Vis spectra of **3** and **6** are identical to those of **2** and **5**, respectively.

The electronic spectra of the compounds present two distinct regions. The first one, below 400 nm, is rather similar for the Ni, Cu or Zn compounds (Figures 12, 13, S4 and S5). In the solid state, the absorption bands in this region clearly saturate, which prevents the resolution of the various bands. They can be attributed to $\pi\rightarrow\pi^*$ and $n\rightarrow\pi^*$ transitions originating from the C=N groups or from the benzene rings and to metal-to-ligand charge-transfer transitions

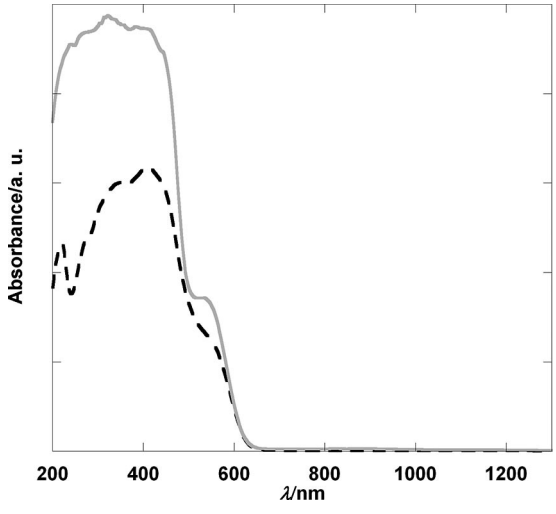

Figure 12. Solid-state UV/Vis spectra of $[Ni(SalenSO_3)]Na_2$ (**1**) (grey solid line) and $[Ni((R,R)CySalenSO_3)]NaK$ (**2**) (black dashed line).

(d→π*).[50–52] For chiral compounds **2**, **3**, **5**, **6** and **8**, the CD spectra bring some more information in the high-energy region, by evidencing a transition showing a strong CD signal, centred at 410 nm for **2** and **3** (Figure 14), at 385 nm for **5** and **6** (Figure 15) and at 370 nm for **9** (Figure S7). This transition can be attributed to a ligand-centred transition, as can be seen from the CD spectra of the ligands alone where a transition occurs at 415 nm, attributed to a n→π* transition (Figure S5). For the chiral Ni compounds **2** and **3**, an additional transition at 480 nm is identified with a rather important CD signal. This transition may be attributed to a metal-to-ligand charge-transfer transition (d→π*).[50,53–55] In the lower-energy region, one band, absent in the spectra of the free ligands (see Figure S5), appears clearly at 530 nm for the Ni compounds, associated with a very weak CD signal for **2** and **3**. As described in other studies on square-planar Ni^{II} Schiff base complexes, this band can be attributed to the $d_{xy}\rightarrow d_{x2-y2}$ ($^1A_1\rightarrow{}^1B_1$ assuming a C_{2v} symmetry) transition.[50] For the copper compounds, a broad band appears in the visible region, between 500 and 1000 nm, as often observed for Cu^{II} complexes and corresponding to d–d transitions.[53] This band is clearly formed by several transitions, whose relative intensities vary: for **8** and **9** there are at least two transitions of comparable intensity, one around 590 nm, the other around 800 nm (Figure 13), whereas for **4**, **5** and **6**, the intensity of the low-energy transition is much smaller than the other (Figure S4). This difference is probably due to a difference in the symmetry of the Cu^{II} coordination site, but the absence of crystal structures for **4**, **5** and **6** prevents any further rationalization.

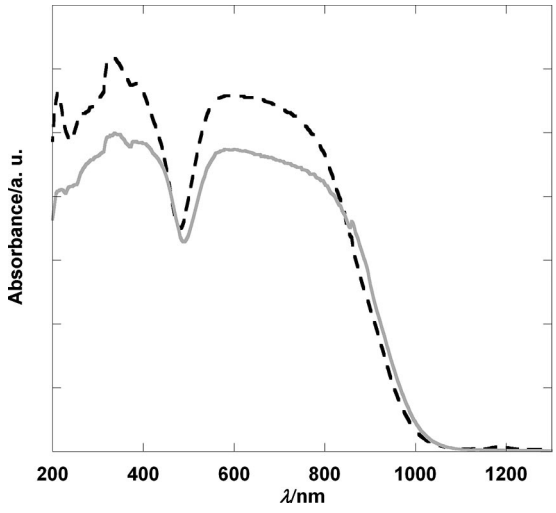

Figure 13. Solid-state UV/Vis spectra of $Cu(SalSO_3)$ (**8**) (grey solid line) and $Cu((R,R)CySalSO_3)$ (**9**) (black dashed line).

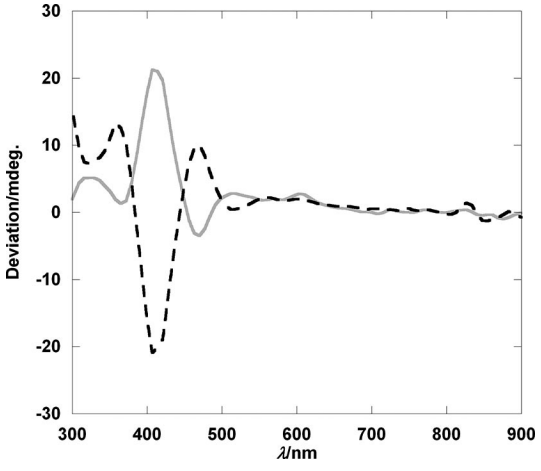

Figure 14. Solid-state CD spectra of $[Ni((R,R)CySalenSO_3)]Na_2$ (**2**) (black dashed line) and $[Ni((S,S)CySalenSO_3)]Na_2$ (**3**) (grey solid line).

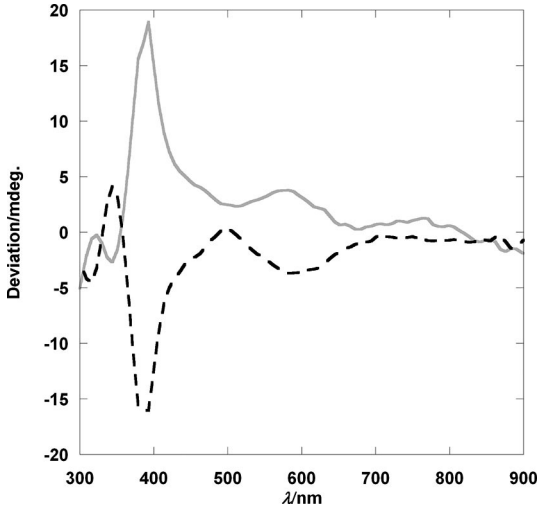

Figure 15. Solid-state CD spectra of $[Cu((R,R)CySalenSO_3)]Na_2$ (**5**) (black dashed line) and $[Cu((S,S)CySalenSO_3)]Na_2$ (**6**) (grey solid line).

Magnetic Study

The magnetic properties of the compounds were investigated by SQUID magnetometry. As expected for square-planar Ni^{II} complexes, nickel compounds **1**, **2** and **3** are diamagnetic. Cu^{II} compounds **4**, **5** and **6** behave as paramagnetic species with Curie constant values in accordance with what is expected for Cu^{II} ions [0.43 and 0.42 emu K mol^{-1} for **4** and **5** (and **6**), respectively]. The presence of intermolecular antiferromagnetic interactions can be evidenced by the decrease of the χT product when decreasing the temperature (Figure S8).

The evolution of the χT product as a function of temperature for **8** and **9** is represented in Figure 16. For both compounds the inverse of the susceptibility varies linearly with the temperature (above 200 K) and can be fitted by the Curie–Weiss law, giving C = 0.39 emu K mol^{-1} and 0.41 emu K mol^{-1} for **8** and **9**, respectively, in agreement with the expected value for one Cu^{II} ion. In both cases, the χT product remains constant when decreasing the temperature till about 100 K. Below this value, $\chi T(T)$ for **8** starts increasing continuously, up to 0.46 emu K mol^{-1} at 2 K, indicating ferromagnetic interactions. For **9**, on the contrary, $\chi T(T)$ decreases below 100 K, reaching 0.16 emu K mol^{-1} at 2 K, pointing out antiferromagnetic interactions.

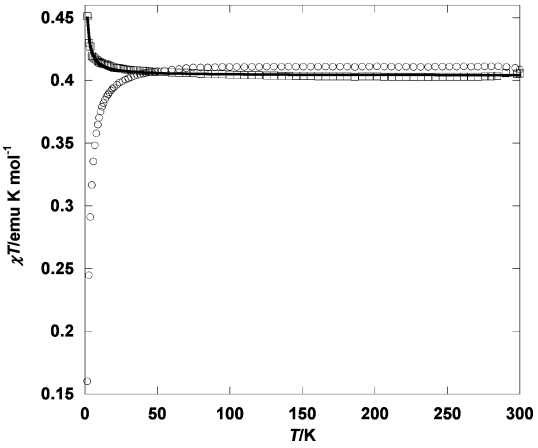

Figure 16. Magnetic behaviour of [Cu(SalSO$_3$)] (**8**) (squares) and [Cu((*R*,*R*)CySalSO$_3$)] (**9**) (circles). Solid line represents the best fit (see text).

In the case of **9**, the observed antiferromagnetic behaviour is attributed to intermolecular interactions between mononuclear Cu^{II} complexes, which can be mediated by hydrogen bonds, for instance. In the molecular field approach, these intermolecular antiferromagnetic interactions can be identified with the Weiss temperature, θ = –0.87 K, deduced from the fit of the inverse susceptibility to the Curie–Weiss law.

After examination of the structure of **8**, its magnetic behaviour can be understood by considering Cu(SalSO$_3$) dimers, with ferromagnetic intradimer interaction through the ligand. The χT = f(T) and χ = f(T) curves can be fitted with the spin Hamiltonian $\hat{H} = -J\hat{\mathbf{S}}_{\mathbf{Cu1}}\hat{\mathbf{S}}_{\mathbf{Cu2}} + g\beta\mathbf{H}\hat{\mathbf{S}}$, in which all parameters have their usual meaning and the spin operator $\hat{\mathbf{S}}$ is defined as $\hat{\mathbf{S}} = \hat{\mathbf{S}}_{\mathbf{Cu1}} + \hat{\mathbf{S}}_{\mathbf{Cu2}}$.

The fit leads to the following values: J = 0.66(1) cm^{-1}, g = 2.08(1) with an excellent agreement factor $R = 1.3 \times 10^{-5}$. As expected from the Cu–Cu distance, the exchange constant is very small. To understand the microscopic origins of this small ferromagnetic interaction, a theoretical approach is very much needed.

Therefore, in order to get a direct insight into the local electronic structure and, in particular, into the spin distribution of the structure of **8**, we performed first principles calculations within the density functional theory (DFT) approach.[56] We adopted a plane wave (PW) basis set with a cut-off of 80 Ry and we described the core-valence interaction by means of norm-conserving Trouiller–Martins pseudopotentials.[57] To eliminate the spurious interactions with periodically repeated images of the system, induced by the use of periodic boundary conditions, typical of PW approaches, we dumped the wavefunctions outside the border of the simulation cell according to the Barnett–Landman scheme for the treatment of isolated systems.[58] The delicate point in DFT calculations for this class of systems is represented by the choice of the exchange and correlation functionals, which can lead to results moderately depending on the type of generalized gradient approximations used.[59] To address, at least partially, this issue, we performed the calculations by using two types of gradient corrections: (a) the Becke[60] and Lee–Parr–Yang[61] (BLYP) for the exchange and correlation functionals, respectively and (b) the Hamprecht–Cohen–Tozer–Handy (HCTH) functional.[62] All these calculations were performed with the CPMD package.[63] The results are highlighted in Figure 17, referring to the BLYP calculations, where the spin density distribution is shown in terms of isosurfaces at values of 2×10^{-4} and 2×10^{-5} e Å^{-3} (the ferromagnetic BLYP result is displayed). From the standpoint of the considerations that will be developed hereafter on the spatial extension of the spin densities, no substantial differences exist between the BLYP and the HCTH cases. We obtained total energy differences between the ferromagnetic and the antiferromagnetic solutions equal to 32 cm^{-1} and 20 cm^{-1} for the BLYP and HCTH cases, respectively, the lowest energy being associated with the ferromagnetic solution. These rather small differences are consistent with the above measurements [experimentally J = +0.66(1) cm^{-1}] and can be tentatively ascribed to the presence of a sulfonato SO$_3$ group, experimentally known for being a ligand hampering efficient magnetic coupling.[64] Coming to the spin density distribution, we can observe that, in the ferromagnetic solution, the major contributions appear localized on the Cu atoms and on the surrounding sites, namely the O and N atoms directly coordinated by the metal atom. A path of spin densities connecting the Cu centres and extending into the SO$_3$ group becomes visible only at very low values (2×10^{-5} e Å^{-3}), where a spin distribution along the S–C bond becomes visible. This provides convincing evidence of the very limited (essentially vanishing) extent of the magnetic coupling within this complex.

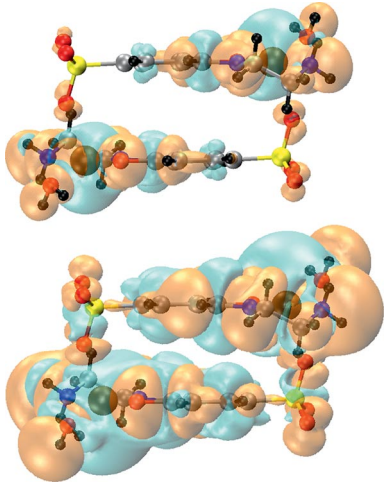

Figure 17. Isosurfaces of spin density values [blue and light brown colours indicating α (up) and β (down) spin populations, respectively]. Top: isosurfaces at 2×10^{-4} e Å^{-3}. Bottom: isosurfaces at 2×10^{-5} e Å^{-3}. The software VMD is used for the graphic presentation of the results.[65]

Conclusions

We have reported here and fully characterized five new sulfonato salen complexes, two of which are chiral. The

crystal structures of the Ni complexes have been solved, as well as those of three other compounds resulting from the partial hydrolysis of the complexes. On the basis of these structures, which enlarge the rather small family of structures of compounds bearing sulfonato groups, we have been able to draw a general correlation between the position of the infrared absorption bands of sulfonato groups and their coordination mode. Finally the magnetic properties of a sulfonato-bridged copper(II) dinuclear complex have been investigated, revealing unexpected and very small ferromagnetic interaction between the two copper(II) ions. DFT calculations have shown that spin densities alternating along the ligand and slightly extending though the sulfonato groups couple the two copper(II) ions.

Experimental Section

General Remarks

Salicylaldehyde, aniline, *trans*-diaminocyclohexane, ethylenediamine and metal salts were purchased from Alfa-Aesar, Acros and Fluka and were used as received.

Elemental analyses for C, H, N, S, Co and Cu were carried out at the Service Central d'Analyse of the CNRS (USR-59). FTIR spectra were collected with a Digilab FTS 3000 computer-driven instrument (0.1 mm thick powder samples in KBr). ^{1}H NMR spectra were recorded with a Bruker AVANCE 300 (300 MHz) spectrometer. The internal references of the spectrum correspond to the peak of the nondeuteriated solvent. UV/Vis/NIR studies were performed with a Perkin–Elmer Lambda 950 spectrometer (spectra recorded in the reflection mode, by using a 150 mm integrating sphere, with a mean resolution of 2 nm and a mean sampling rate of 300 nm min^{-1}). Circular dichroism was measured with a Jasco 810 spectrometer. The magnetic studies were carried out with a SQUID magnetometer (Quantum Design MPMS-*XL*) covering the temperature and field ranges 2–300 K, ± 5 T; ac susceptibility measurements were performed in a 0.35 mT alternative field (100 Hz). Magnetization measurements at different fields at room temperature confirm the absence of ferromagnetic impurities, and data were corrected for diamagnetic contributions of the samples and of the sample holder.

Crystal Structure Determinations

Single crystals of ligand **A**, complexes **1′**, **2**, **8** and **9** were mounted on a Nonius Kappa-CCD area detector diffractometer (Mo-K_α λ = 0.71073 Å). The complete conditions of data collection (Denzo software[66]) and structure refinements are given in Tables 2 and S1. A list of hydrogen bonds is also given in Tables S1 to S5. The cell parameters were determined from reflections taken from one set of 10 frames (1.0° steps in phi angle), each at 20 s exposure. The structures were solved by direct methods (SHELXS97) and refined against F^2 by using the SHELXL97 and CRYSTALBUILDER softwares.[67,68] The absorption was not corrected. All non-hydrogen atoms were refined anisotropically except the O in H_2O solvent molecules. Hydrogen atoms were generated according to stereochemistry and refined by using a riding model in SHELXL97. CCDC-757612, -757613, -757614, -757615, -757616 contain the supplementary crystallographic data for this paper. These data can be obtained free of charge from The Cambridge Crystallographic Data Centre via www.ccdc.cam.ac.uk/data_request/cif.

Table 2. Crystal data and refinement details for **A**, **1′**, **2**, **8** and **9**.

	A	**1′**	**2**	**8**	**9**
Formula	$C_7H_5NaO_5S\cdot H_2O$	$(C_{16}H_{12}N_2NiO_8S_2)_4Na_7\cdot 8H_2O\cdot 14O$[a]	$C_{20}H_{18}KN_2NaNiO_8S_2\cdot 5H_2O$	$(C_9H_{10}CuN_2O_4S)_2\cdot 2H_2O$	$(C_{13}H_{16}CuN_4O_8S)_2\cdot 6H_2O$
Formula weight	242.18	2461.48	689.36	647.61	827.85
Crystal system	monoclinic	triclinic	monoclinic	monoclinic	triclinic
Space group	$P2_1/a$ (No. 14)	$P\bar{1}$ (No. 2)	$P2_1$ (No. 4)	$P2_1/n$ (No. 14)	$P1$ (No. 1)
a /Å	6.143(4)	13.3760(10)	11.8260(9)	7.507(5)	9.392(3)
b /Å	22.191(9)	13.6210(10)	6.8820(3)	10.330(5)	9.684(3)
c /Å	6.745(4)	15.0400(10)	18.5710(13)	14.714(8)	10.706(3)
α /°	90	68.16(2)	90	90	64.21(2)
β /°	98.43(3)	80.03(2)	91.256(3)	95.79(3)	76.24(2)
γ /°	90	82.74(2)	90	90	72.65(2)
V /Å^3	909.5(9)	2499.4(5)	1511.07(17)	1135.2(11)	830.2(5)
Z	4	1	2	2	1
d(calc) /g cm^{-3}	1.769	1.635	1.515	1.895	1.656
μ(Mo-K_α) /mm^{-1}	0.408	1.042	0.994	2.123	1.480
F(000)	496	1253	712	660	430
Crystal size /mm	0.10 × 0.10 × 0.10	0.10 × 0.10 × 0.10	0.10 × 0.10 × 0.10	0.08 × 0.08 × 0.20	0.10 × 0.12 × 0.15
Temperature /K	173	173	173	173	173
$\theta_{min\text{-}max}$ /°	1.8–30.0	1.5–27.1	1.1–30.0	2.4–30.0	2.1–30.0
Data set	–8/8; –25/31, –9/7	–16/17; –15/17; 0/19	–16/12; –6/9, –25/26	–8/10; –14/12; –14/20	–16/12; –6/9; –25/26
Total, unique data, R(int)	6351, 2656, 0.111	11006, 11006, 0.059	11575, 7782, 0.068	7399, 3303, 0.080	11694, 7175, 0.061
Obs. data [$I > 2.0\sigma(I)$]	1491	9237	5499	2649	6438
Refinement					
N_{ref}, N_{par}	2656, 147	11006, 624	7782, 379	3303, 176	7175, 433
R, $wR2$, S	0.0620, 0.1927, 1.03	0.0754, 0.2306, 1.04	0.0726, 0.1828, 1.07	0.0513, 0.1332, 1.07	0.0512, 0.1525, 1.03
Max. and Av. shift/error	0.00, 0.00	0.00, 0.00	0.03, 0.00	0.00, 0.00	0.00, 0.00
Flack x	–	–	0.05(2)	–	0.02(12)
Min. and Max. resd. dens. /e Å^{-3}	–0.78, 0.41	–1.00, 2.58	–0.87, 1.04	–1.16, 0.89	–1.11, 0.60

[a] The 14 O atoms correspond to uncoordinated water molecules; the accuracy of the diffraction data was not sufficient to locate H atoms (see text).

EurJIC European Journal of Inorganic Chemistry

Synthesis of Complexes

The syntheses of 5-sulfosalicylaldehyde sodium salt (**A**),[33,34] (*R*,*R*) 1,2-diammoniumcyclohexane mono-(+)-tartrate (**D**)[69] and (*S*,*S*) 1,2-diammoniumcyclohexane bis(+)-monohydrogenotartrate (**E**)[70] were adapted from published procedures. Crystals of **A** were obtained by slow evaporation of a solution of water and ethanol (1:1 v/v) containing [Zn(SalenSO$_3$)Na$_2$] (**7**) (see below) (10 mg in 10 mL of solution) in about three weeks.

Bis(5-sulfonatosalicylaldehyde)nickel(II) Disodium Salt (B): The procedure is adapted from ref.[42]. 5-Sulfonatosalicylaldehyde sodium salt (**A**) (3.3 g, 14.6 mmol) was dissolved in an aqueous solution of sodium hydroxide (15 mL, 1 M). An aqueous solution of $NiCl_2·6H_2O$ (1.75 g, 7.4 mmol, dissolved in 5 mL of water) was then added slowly to the solution. The solution that was initially yellow became dark green, and after one hour of agitation, a pea green solid formed. The solid was filtered, washed with water and ethanol and dried under vacuum. Yield 85–90%. **B**·6H$_2$O ($C_{14}H_8Na_2NiO_{10}S_2·6H_2O$, 613.10): calcd. C 27.43, H 3.29, S 10.46, Ni 9.57; found C 27.14, H 3.24, S 9.82, Ni 10.02. IR (KBr pellet): $\tilde{\nu}$ = 3585 (m), 3518 (m), 3422 (m), 2878 (w), 2790 (w), 1651 (s), 1524 (s), 1466 (s), 1405 (m), 1336 (w), 1204 (s), 1171 (s), 1124 (s), 1045 (s), 922 (w), 840 (w), 755 (w), 678 (m), 621 (m), 532 (w) cm^{-1}.

***N*,*N*′-Bis(5-sulfonatosalicylidene)-1,2-diaminoethane Disodium Salt (SalenSO$_3$)Na$_2$ (C):** 5-Sulfonatosalicylaldehyde sodium salt (**A**) (2.24 g, 10 mmol) was poured into ethanol (50 mL). Ethylenediamine (300 mg, 0.33 mL, 5 mmol) was then added and the mixture turned yellow. The mixture was heated at 90 °C for one hour. The yellow solid was filtered, washed with ethanol and dried in vacuo. Yield 80%. **C**·H$_2$O ($C_{16}H_{14}N_2Na_2O_8S_2·H_2O$, 490.42): calcd. C 39.19, H 3.29, N 5.71; found C 39.39, H 3.41, N 5.33. ^{1}H NMR ([D$_6$]DMSO): δ = 8.65 (s, 1), 7.67 (d, J = 2.2 Hz, 1 H), 7.51 (dd, J = 2.2, 8.5 Hz, 1 H), 6.78 (d, J = 8.5 Hz, 1 H), 3.91 (s, 2 H) ppm. IR (KBr pellet): $\tilde{\nu}$ = 3443 (w), 2963 (w), 2894 (w), 1637 (s), 1613 (m), 1580 (m), 1484 (m), 1397 (w), 1359 (w), 1295 (m), 1234 (s), 1187 (s), 1116 (s), 1054 (s), 1035 (s), 906 (w), 893 (w), 844 (m), 802 (m), 733 (w), 662 (m), 604 (s) cm^{-1}.

(*R*,*R*)-*N*,*N*′-Bis(5-sulfonatosalicylidene)-1,2-diaminocyclohexane Sodium–Potassium Salt {[(*R*,*R*)CySalenSO$_3$]NaK} (F): D (2.97 g, 11.3 mmol) and K_2CO_3 (3.12 g, 22.6 mmol) were dissolved in an ethanol/water (1:4 v/v) solution (20 mL) in a two-necked round-bottomed flask with a reflux condenser and an addition funnel. The mixture was heated for one hour at 100 °C. Then an aqueous solution of **A** (36 mL, 0.68 M) was added slowly. The yellow solution was heated for two hours at 100 °C. The volume of the solution was reduced to one half by rotary evaporation, and ethanol was added until a yellow precipitate formed. The solid was filtered, washed with ethanol and dried in vacuo. Yield 90%. ^{1}H NMR ([D$_6$]DMSO): δ = 8.57 (s, 1 H), 7.61 (d, J = 2.2 Hz, 1 H), 7.45 (dd, J = 2.2, 8.5 Hz, 1 H), 6.71 (d, J = 8.5 Hz, 1 H), 3.42 (m, 1 H), 1.70 (m, 4 H) ppm. IR (KBr pellet): $\tilde{\nu}$ = 3404 (s), 2936 (w), 2862 (w), 1630 (s), 1606 (s), 1518 (m), 1478 (m), 1463 (m), 1408 (m), 1379 (m), 1352 (m), 1285 (w), 1194 (s), 1177 (s), 1107 (s), 1033 (s), 916 (m), 841 (m), 731 (w), 708 (w), 670 (m), 603 (m), 561 (w), 519 (w), 483 (w), 447 (w) cm^{-1}. $[\alpha]_D^{20}$ = +37°·(DMSO).

(*S*,*S*)-*N*,*N*′-Bis(5-sulfonatosalicylidene)-1,2-diaminocyclohexane Disodium Salt [((*S*,*S*)CySalenSO$_3$)NaK] (G): The same procedure as above was used but **D** was replaced by **E**. ^{1}H NMR ([D$_6$]DMSO): δ = 8.56 (s, 1 H), 7.61 (d, J = 2.2 Hz, 1 H), 7.45 (dd, J = 2.2, 8.5 Hz, 1 H), 6.69 (d, J = 8.5 Hz, 1 H), 3.43 (m, 1 H), 1.70 (m, 4 H) ppm. IR (KBr pellet): $\tilde{\nu}$ = 3406 (s), 2935 (w), 2861 (w), 1632 (s), 1610 (s), 1522 (m), 1473 (m), 1380 (m), 1286 (w), 1158 (s), 1108 (s), 1034 (s), 949 (m), 916 (m), 835 (m), 727 (w), 706 (w), 670 (m), 600 (m), 562 (w), 468 (w) cm^{-1}. $[\alpha]_D^{20}$ = –44° (DMSO).

Bis(5-sulfonatosalicylaldehyde)zinc(II) Disodium Salt (H): (Adapted from ref.[42]) 5-Sulfonatosalicylaldehyde sodium salt (**A**) (3.3 g, 14.6 mmol) was dissolved in an aqueous solution of sodium hydroxide (15 mL, 1 M). An aqueous solution of $ZnCl_2$ (1.00 g, 7.3 mmol, dissolved in 5 mL of water) was then added slowly to the solution. After stirring for one hour at room temperature, a white solid formed. The solid was filtered, washed with water and ethanol and dried under vacuum. Yield 80–85%. **H**·3H$_2$O ($C_{14}H_8Na_2O_{10}S_2Zn·3H_2O$, 565.75): C 29.72, H 2.49, S 11.34, Na 8.13, Zn 11.56; found C 28.23, H 2.00, S 10.38, Na 8.27, Zn 14.10. ^{1}H NMR ([D$_6$]DMSO): δ = 9.51 (s, 1 H), 7.62 (d, J = 2.5 Hz, 1 H), 7.49 (dd, J = 2.5, 8.7 Hz, 1 H), 6.55 (d, J = 8.7 Hz, 1 H) ppm. IR (KBr pellet): $\tilde{\nu}$ = 3585 (m), 3519 (m), 3218 (m), 2872 (w), 2785 (w), 1651 (s), 1525 (m), 1463 (s), 1406 (m), 13356 (w), 1171 (s), 1122 (s), 1043 (s), 921 (w), 841 (w), 753 (w), 676 (m), 615 (m), 518 (w), 451 (w) cm^{-1}.

***N*,*N*′-Bis(5-sulfonatosalicylidene)-1,2-diaminoethanenickel(II) Disodium Salt [Ni(SalenSO$_3$)Na$_2$] (1):** (Adapted from ref.[33]) Ethylenediamine (99 μL, 1.5 mmol) was added to a mixture of water (4.5 mL) and ethanol (30 mL) previously degassed for 15 min. Bis(5-sulfonatosalicylaldehyde)nickel(II) disodium salt (**B**) (837 mg, 1.5 mmol) was introduced, and the mixture was stirred for one hour at 90 °C. The orange solid was filtered, washed with ethanol and dried under vacuum. Yield 70%. Ni(SalenSO$_3$)Na$_2$·3H$_2$O ($C_{16}H_{12}N_2Na_2NiO_8S_2·3H_2O$, 581.85): Ni 10.07, C 32.96, H 3.11, N 4.80, S 11.00, Na 7.89; found Ni 10.47, C 33.07, H 3.00, N 4.38, S 10.77, Na 8.21. ^{1}H NMR ([D$_6$]DMSO): δ = 7.95 (s, 1 H), 7.55 (s, 1 H), 7.35 (d, J = 8.4 Hz, 1 H), 6.65 (d, J = 8.4 Hz, 1 H), 3.45 (s, 2 H) ppm. IR (KBr pellet): $\tilde{\nu}$ = 3568 (m), 3517 (m), 3460 (m), 3277 (w), 3221 (w), 3138 (w), 1650 (s), 1617 (s), 1534 (s), 1468 (s), 1384 (w), 1337 (w), 1205 (s), 1173 (s), 1116 (s), 1042 (s), 951 (w), 839 (w), 817 (w), 741 (w), 681 (w), 635 (m), 610 (m), 531 (w), 467 (w) cm^{-1}. Partially protonated crystals of **1** {**1**′: [Ni(SalenSO$_3$)]$_8$Na$_7$·22H$_2$O plus one nonlocalized H$^+$} were obtained by slow evaporation of a solution of water and ethanol (1:1 v/v) containing Ni(SalenSO$_3$)Na$_2$ (**1**) (10 mg in 10 mL of solution) in about four months.

(*R*,*R*)-*N*,*N*′-Bis(5-sulfonatosalicylidene)-1,2-diaminocyclohexanenickel(II) Sodium–Potassium Salt [Ni((*R*,*R*)CySalenSO$_3$)NaK] (2): ((*R*,*R*)CySalenSO$_3$)NaK (**F**) (2.63 g, 4.9 mmol) was dissolved in a mixture of water/ethanol (50 mL, 1:1 v/v) in a two-necked round-bottomed flask with a condenser and an addition funnel. Then $NiCl_2·6H_2O$ (1.18 g, 5.0 mmol) dissolved in a mixture of water/ethanol (50 mL, 1:1 v/v) was slowly added. The mixture was heated to reflux for 1 h. The hot solution was filtered, and the filtrate was cooled with an ice bath. Then ethanol was added until an orange solid formed. The solid was filtered and washed with ethanol. Yield 50–55%. Ni((*R*,*R*)CySalenSO$_3$)NaK·3H$_2$O ($C_{20}H_{18}KN_2NaNiO_8S_2·3H_2O$, 652.44): C 36.82, H 3.71, N 4.29, Na 3.52, Ni 9.00; found C 36.86, H 3.50, N 4.39, Na 2.59, Ni 9.59. ^{1}H NMR ([D$_6$]DMSO): δ = 7.75 (s, 2 H), 7.65 (s, 2 H), 7.35 (d, J = 2 H, 8.5 Hz), 6.60 (d, J = 2 H, 8.5 Hz), 3.5 (m, 2 H), 3.1 (s, 2 H), 1.75 (s, 2 H), 1.25 (s, 4 H) ppm. IR (KBr pellet): $\tilde{\nu}$ = 3447 (m), 2937 (w), 2864 (w), 1624 (s), 1601 (s), 1559 (w), 1533 (m), 1466 (m), 1423 (w), 1381 (w), 1343 (w), 1324 (w), 1209 (sh), 1178 (s), 1109 (s), 1032 (s), 933 (w), 890 (w), 830 (w), 751 (w), 688 (m), 619 (s), 578 (m), 557 (w), 530 (w), 449 (w) cm^{-1}. $[\alpha]_D^{20}$ = –230° (H$_2$O). Crystals were obtained by slow diffusion of 2-propanol (5 mL) in an aqueous solution (5 mL) of Ni((*R*,*R*)CySalenSO$_3$)NaK (**2**) (10 mg), in about one month.

(*S*,*S*)-*N*,*N*′-Bis(5-sulfonatosalicylidene)-1,2-diaminocyclohexanenickel(II) Sodium–Potassium Salt [Ni((*S*,*S*)CySalenSO$_3$)NaK] (3):

The same procedure as above was used but **F** was replaced by **G**. Yield 50–55%. Ni((*S*,*S*)CySalenSO$_3$)NaK·3H$_2$O ($C_{20}H_{18}KN_2NaNiO_8S_2$·3H$_2$O, 652.44): C 36.82, H 3.71, N 4.29, Na 3.52, Ni 9.00; C 36.87, H 3.50, N 4.36, Na 2.72, Ni 8.97. ^{1}H NMR and IR spectra are identical to those of **2**. $[\alpha]_D^{20}$ = +200° (H$_2$O).

***N*,*N*′-Bis(5-sulfonatosalicylidene)-1,2-diaminoethanecopper(II) Disodium Salt [Cu(SalenSO$_3$)Na$_2$] (4):** **C** (1.42 g, 2.9 mmol) was dissolved in a water/ethanol mixture (50 mL, 1:1 v/v) in a two-necked round-bottomed flask with a condenser and an addition funnel. Then 50 mL of a water/ethanol (1:1 v/v) solution of Cu(OAc)$_2$·H$_2$O (0.599 g, 3.0 mmol) was slowly added. The mixture was heated for one hour at reflux. The hot solution was filtered and cooled with an ice bath. Then ethanol was added, and a violet solid precipitated. The solid was filtered and washed with ethanol. Yield 50–55%. Cu(SalenSO$_3$)Na$_2$·5H$_2$O ($C_{16}H_{12}CuN_2Na_2O_8S_2$·5H$_2$O, 624.00): C 30.80, H 3.55, N 4.49, S 10.28, Cu 10.18, Na 7.37; found C 30.50, H 3.70, N 4.99, S 10.36, Cu 10.80, Na 7.28. IR (KBr pellet): $\tilde{\nu}$ = 3453 (s), 1641 (s), 1602 (m), 1534 (m), 1465 (m), 1382 (m), 1333 (m), 1312 (m), 1191 (s), 1174 (s), 1117 (s), 1033 (s), 972 (w), 931 (w), 893 (w), 832 (m), 793 (w), 738 (w), 672 (m), 623 (m), 600 (m), 525 (w), 460 (w), 408 (w) cm^{-1}.

(*R*,*R*)-*N*,*N*′-Bis(5-sulfonatosalicylidene)-1,2-diaminocyclohexanecopper(II) Sodium–Potassium Salt [Cu((*R*,*R*)CySalenSO$_3$)NaK] (5): **F** (2.63 g, 4.9 mmol) was dissolved in a mixture of water/ethanol (20 mL, 1:1 v/v) in a two-necked round-bottomed flask with a condenser and an addition funnel. Then Cu(OAc)$_2$·H$_2$O (0.99 g, 5.0 mmol) dissolved in a mixture of water/ethanol (80 mL, 1:1 v/v) was slowly added. The mixture was heated to reflux for 1 h. The hot solution was filtered and the filtrate was cooled with an ice bath. Then ethanol was added until a blue solid formed. The solid was filtered and washed with ethanol. Yield 50–55%. Cu((*R*,*R*)CySalenSO$_3$)NaK·6H$_2$O ($C_{20}H_{18}CuKN_2NaO_8S_2$·6H$_2$O, 712.22): C 33.73, H 4.25, N 3.93, S 9.00, Na 3.23, Cu 8.92; found C 33.36, H 4.51, N 3.69, S 8.59, Na 2.65, Cu 9.36. IR (KBr pellet): $\tilde{\nu}$ = 3447 (s), 2940 (w), 2854 (w), 1635 (s), 1598 (s), 1528 (m), 1465 (m), 1420 (w), 1384 (m), 1353 (m), 1319 (m), 1183 (s), 1113 (s), 1031 (s), 972 (w), 930 (w), 893 (w), 838 (m), 803 (w), 748 (w), 681 (m), 614 (m), 568 (w), 513 (w), 461 (w), 417 (w) cm^{-1}.

(*S*,*S*)-*N*,*N*′-Bis(5-sulfonatosalicylidene)-1,2-diaminocyclohexanecopper(II) Sodium–Potassium Salt [Cu((*S*,*S*)CySalenSO$_3$)NaK] (6): The same procedure as above was used but **F** was replaced by **G**. Yield 50–55%. IR (KBr pellet): $\tilde{\nu}$ = 3447 (s), 2940 (w), 2854 (w), 1635 (s), 1598 (s), 1528 (m), 1465 (m), 1420 (w), 1384 (m), 1353 (m), 1319 (m), 1183 (s), 1113 (s), 1031 (s), 972 (w), 930 (w), 893 (w), 838 (m), 803 (w), 748 (w), 681 (m), 614 (m), 568 (w), 513 (w), 461 (w), 417 (w) cm^{-1}.

***N*,*N*′-Bis(5-sulfonatosalicylidene)-1,2-diaminoethanezinc(II) Disodium Salt [Zn(SalenSO$_3$)Na$_2$] (7):** Ethylenediamine (99 μL, 1.5 mmol) was added to a mixture of ethanol (30 mL) and water (4.5 mL) previously degassed for 15 min. Bis(5-sulfonatosalicylaldehyde)zinc(II) disodium salt (**H**) (837 mg, 1.4 mmol) was introduced, and the mixture was stirred for one hour at 90 °C. The white solid was filtered, washed with ethanol and dried under vacuum. Yield 70%. Zn(SalenSO$_3$)Na$_2$·4H$_2$O ($C_{16}H_{12}N_2Na_2O_8S_2Zn$·4H$_2$O, 607.84): C 31.62, H 3.32, N 4.61, S 10.55, Zn 10.76, Na 7.56; found C 31.56, H 3.37, N 4.71, S 10.12, Zn 11.11, Na 7.31. ^{1}H NMR ([D$_6$]DMSO): δ = 8.43 (s, 1 H), 7.41 (d, J = 2.4 Hz, 1 H), 7.32 (dd, J = 2.4, 8.8 Hz, 1 H), 6.52 (d, J = 8.8 Hz, 1 H), 3.72 (s, 2 H) ppm. IR (KBr pellet): $\tilde{\nu}$ = 3604 (s), 3523 (s), 3447 (m), 1641 (s), 1601 (m), 1537 (s), 1472 (s), 1382 (m), 1341 (m), 1312 (m), 1205 (s), 1169 (s), 1123 (s), 1045 (s), 986 (w), 945 (w), 931 (w), 901 (w), 833 (m), 792 (w), 739 (m), 669 (m), 621 (m), 567 (w), 567 (w), 539 (w), 465 (w), 406 (w) cm^{-1}.

***N*-(5-Sulfonatosalicylidene)-1,2-diaminoethanecopper(II) [Cu(SalSO$_3$)] (8):** Crystals were obtained by slow evaporation of the filtrate of the synthesis of Cu(SalenSO$_3$)Na$_2$ (**4**) in about one month. Cu(SalSO$_3$)·H$_2$O ($C_9H_{10}CuN_2O_4S$·H$_2$O, 323.81): C 33.38, H 3.74, N 8.65; found C 33.13, H 3.73, N 8.69. IR (KBr pellet): $\tilde{\nu}$ = 3278 (m), 3240 (m), 3155 (m), 2920 (w), 2858 (w), 1648 (s), 1600 (m), 1559 (w), 1525 (m), 1466 (m), 1387 (m), 1330 (m), 1261 (vw), 1194 (s), 1112 (s), 1034 (s), 918 (w), 837 (m), 729 (w), 691 (w), 667 (w), 611 (s), 538 (w), 486 (w), 470 (w), 421 (w) cm^{-1}.

(*R*,*R*)-*N*-(5-Sulfonatosalicylidene)-1,2-diaminocyclohexanecopper(II) [Cu((*R*,*R*)CySalSO$_3$)] (9): Crystals were obtained by slow evaporation of the filtrate of the synthesis of Cu((*R*,*R*)CySalenSO$_3$)NaK (**5**) in about one month. Cu((*R*,*R*)CySalSO$_3$)·3H$_2$O ($C_{13}H_{16}CuN_2O_4S$·3H$_2$O, 413.94): C 37.72, H 5.36, N 6.77; found C 37.51, H 5.31, N 6.79. IR (KBr pellet): $\tilde{\nu}$ = 3548 (m), 3313 (m), 3243 (w), 3161 (w), 2948 (w), 2863 (w), 1639 (s), 1595 (m), 1560 (w), 1532 (m), 1470 (m), 1387 (m), 1338 (w), 1317 (w), 1190 (s), 1119 (s), 1034 (s), 923 (w), 834 (w), 748 (w), 724 (w), 681 (w), 610 (m), 575 (w), 526 (w), 502 (w), 457 (w) cm^{-1}.

Supporting Information (see footnote on the first page of this article): List of hydrogen bonds determined by PLATON for **A**, **1**′, **2**, **8** and **9**, IR spectra of **A**, **1**, **2**, **8** and **9**, UV/Vis spectra for the free ligands, **4**, **5**, **7** and **A**, CD spectra for the free chiral ligands and **9**, χT vs. T curves for **4** and **5**, and magnetization versus field curves for **8** and **9**.

Acknowledgments

The authors thank the Centre National de la Recherche Scientifique (CNRS), the Université de Strasbourg and the Agence Nationale de la Recherche (ANR) (contract n° ANR-06-JCJC-0008) for funding. M. D. thanks the Agence Universitaire de la Francophonie (Senegal) for a visiting grant. The authors thank A. Derory and D. Burger for technical assistance. We acknowledge computational resources provided by the Centre Informatique National de l'Enseignement Supérieur (CINES), the Institut du Développement et des Ressources en Informatique Scientifique (IDRIS) and the Centre d'Études du Calcul Parallèle et de la Visualization of the University of Strasbourg.

[1] J. J. Bozell, B. R. Hames, D. R. Dimmel, *J. Org. Chem.* **2002**, *60*, 2398–2404.
[2] V. S. Kshirsagar, A. C. Garade, R. B. Mane, K. R. Patil, A. Yamaguchi, M. Shirai, C. V. Rode, *Appl. Cat. A* **2009**, *370*, 16–23.
[3] A. M. I. Jayaseeli, S. Rajagopal, *J. Mol. Cat. A* **2009**, *309*, 103–110.
[4] C. Baleizão, H. Garcia, *Chem. Rev.* **2006**, *106*, 3987–4043.
[5] E. N. Jacobsen, W. Zhang, A. R. Muci, J. R. Ecker, L. Deng, *J. Am. Chem. Soc.* **1991**, *113*, 7063–7064.
[6] E. N. Jacobsen, W. Zhang, M. L. Guler, *J. Am. Chem. Soc.* **1991**, *113*, 6703–6704.
[7] L. E. Martinez, J. L. Leighton, D. H. Carsten, E. N. Jacobsen, *J. Am. Chem. Soc.* **2002**, *117*, 5897–5898.
[8] A. M. Jason, J. Wiechang, T. N. SonBinh, *Angew. Chem. Int. Ed.* **2002**, *41*, 2953–2956.
[9] Z. Li, K. R. Conser, E. N. Jacobsen, *J. Am. Chem. Soc.* **2002**, *115*, 5326–5327.
[10] Y. Tamura, T. Uchida, T. Katsuki, *Tetrahedron Lett.* **2003**, *44*, 3301–3303.
[11] B. Saito, T. Katsuki, *Tetrahedron Lett.* **2001**, *42*, 3873–3876.

[12] P. G. Cozzi, *Chem. Soc. Rev.* **2004**, *33*, 410–421.
[13] E. J. Jarson, V. L. Pecoraro, in *Manganese Redox Enzymes* (Ed.: V. L. Pecoraro), VCH Publisher, Inc., New York, pp. 1–28.
[14] P. G. Cozzi, L. S. Dolci, A. Garelli, M. Montalti, L. Prodi, N. Zaccheroni, *New J. Chem.* **2003**, *27*, 692–697.
[15] A. W. Kleij, *Eur. J. Inorg. Chem.* **2009**, 193–205.
[16] R. M. Haak, S. J. Wezenberg, A. W. Kleij, *Chem. Commun.* **2010**, *46*, 2713–2723.
[17] T. Katsuki, *Coord. Chem. Rev.* **1995**, *140*, 189–214.
[18] M. Kojima, H. Taguchi, M. Tsuchimoto, K. Nakajima, *Coord. Chem. Rev.* **2003**, *237*, 183–196.
[19] H. Miyasaka, A. Saitoh, S. Abe, *Coord. Chem. Rev.* **2007**, *251*, 2622–2664.
[20] N. Herron, *Inorg. Chem.* **2002**, *41*, 4714–4717.
[21] M. R. Maurya, S. J. J. Titinchi, S. Chand, *Appl. Cat. A* **2002**, *228*, 177–187.
[22] M. J. Sabater, A. Corma, A. Domenech, V. Fornés, H. García, *Chem. Commun.* **1997**, 1285–1286.
[23] H. Hamdan, V. Navijanti, H. Nur, M. Mohd Nazlan Mohd, *Solid State Sci.* **2005**, *7*, 239–244.
[24] V. Ayala, A. Corma, M. Iglesias, J. A. Rincón, F. Sánchez, *J. Cat.* **2004**, *224*, 170–177.
[25] I. Bar-Nahum, H. Cohen, R. Neumann, *Inorg. Chem.* **2003**, *42*, 3677–3684.
[26] J. Bu, Z. M. A. Judeh, C. B. Ching, S. Kawi, *Cat. Lett.* **2003**, *85*, 183–187.
[27] L. Frunza, H. Kosslick, H. Landmesser, E. Höft, R. Fricke, *J. Mol. Cat. A* **1997**, *123*, 179–187.
[28] J. M. Fraile, J. I. García, J. Massam, J. A. Mayoral, *J. Mol. Cat. A* **1998**, *136*, 47–57.
[29] X. Zhang, H. Zhou, X. Su, X. Chen, C. Yang, J. Qin, M. Inokuchi, *J. Alloys Compd.* **2007**, *432*, 247–252.
[30] R. Kitaura, G. Onoyama, H. Sakamoto, R. Matsuda, S.-i. Noro, S. Kitagawa, *Angew. Chem. Int. Ed.* **2004**, *43*, 2684–2687.
[31] C.-C. Cheng, M.-C. Liu, *Tetrahedron Lett.* **2000**, *41*, 10047–10053.
[32] T. Luts, H. Papp, *Kinet. Catal.* **2007**, *48*, 176–182.
[33] K. J. Berry, F. Moya, K. S. Murray, A. B. van der Bergen, B. O. West, *J. Chem. Soc., Dalton Trans.* **1982**, 109–115.
[34] M. Botsivali, D. F. Evans, P. H. Missen, M. W. Upton, *J. Chem. Soc., Dalton Trans.* **1985**, 1147–1149.
[35] S. Bhattacharjee, T. J. Dines, J. A. Anderson, *J. Cat.* **2004**, *252*, 398–407.
[36] S. Bhattacharjee, J. A. Anderson, *Chem. Commun.* **2004**, 554–555.
[37] S. Bhattacharjee, J. A. Anderson, *J. Mol. Cat.* **2006**, *249*, 103–110.
[38] S. Bhattacharjee, T. J. Dines, J. A. Anderson, *J. Phys. Chem. C* **2008**, *112*, 14124–14130.
[39] C. Bibal, J.-C. Daran, S. Deroover, R. Poli, *Polyhedron* **2010**, *29*, 639–647.
[40] I. Correia, J. C. Pessoa, M. T. Duarte, M. F. Minas da Piedade, T. Jackush, T. Kiss, M. M. C. A. Castro, C. F. G. C. Geraldes, F. Avecilla, *Eur. J. Inorg. Chem.* **2005**, 732–744.
[41] I. Correia, A. Dornyei, T. Jakusch, F. Avecilla, T. Kiss, J. C. Pessoa, *Eur. J. Inorg. Chem.* **2006**, 2819–2830.
[42] G. N. J. Tyson, S. C. Adams, *J. Am. Chem. Soc.* **1940**, *62*, 1228–1229.
[43] A. W. Addison, T. N. Rao, J. Reedijk, J. van Rijn, G. C. Verschoor, *J. Chem. Soc., Dalton Trans.* **1984**, 1348–1356.
[44] N. B. Colthup, L. H. Daly, S. E. Wiberley, *Introduction to Infrared and Raman Spectroscopy, Third Edition*, Academic Press, London, **1990**.
[45] G. B. Deacon, R. J. Phillips, *Coord. Chem. Rev.* **1980**, *33*, 227–250.
[46] C. Dendrinou-Samara, G. Tsotsou, L. V. Ekateriniadou, A. H. Kortsaris, C. P. Raptopoulou, A. Terzis, D. A. Kyriakidis, D. P. Kessissoglou, *J. Inorg. Biochem.* **1998**, *71*, 171–179.
[47] V. Robert, G. Lemercier, *J. Am. Chem. Soc.* **2006**, *128*, 1183–1187.
[48] E. Delahaye, S. Eyele-Mezui, J.-F. Bardeau, C. Leuvrey, L. Mager, P. Rabu, G. Rogez, *J. Mater. Chem.* **2009**, *19*, 6106–6115.
[49] C. Bauer, P. Jacques, A. Kalt, *Chem. Phys. Lett.* **1999**, *307*, 397–406.
[50] B. Bosnich, *J. Am. Chem. Soc.* **1968**, *90*, 627–632.
[51] R. S. Downing, F. L. Urbach, *J. Am. Chem. Soc.* **1969**, *91*, 5977–5983.
[52] R. S. Downing, F. L. Urbach, *J. Am. Chem. Soc.* **1970**, *92*, 5861–5865.
[53] A. B. P. Lever, *Inorganic Electronic Spectroscopy, 2nd Edition*, Elsevier, Amsterdam, **1984**.
[54] J. Tedim, S. Patrício, R. Bessada, R. Morais, R. Sousa, M. B. Marques, C. Freire, *Eur. J. Inorg. Chem.* **2006**, 3425–3433.
[55] S. Di Bella, I. Fragala, I. Ledoux, M. A. Diaz-Garcia, T. J. Marks, *J. Am. Chem. Soc.* **1997**, *119*, 9550–9557.
[56] W. Kohn, L. J. Sham, *Phys. Rev.* **1965**, *140*, A1133–A1138.
[57] N. Troullier, J. L. Martins, *Phys. Rev. B* **1991**, *43*, 1993–2006.
[58] R. N. Barnett, U. Landman, *Phys. Rev. B* **1993**, *48*, 2081–2097.
[59] E. Ruiz, A. Rodriguez-Fortea, J. Tercero, T. Cauchy, C. Massobrio, *J. Chem. Phys.* **2005**, *123*, 074102.
[60] A. D. Becke, *Phys. Rev. A* **1988**, *38*, 3098–3100.
[61] C. Lee, W. Yang, R. G. Parr, *Phys. Rev. B* **1988**, *37*, 785–789.
[62] F. A. Hamprecht, A. J. Cohen, D. J. Tozer, N. C. Handy, *J. Chem. Phys.* **1998**, *109*, 6264.
[63] *CPMD*, Copyright IBM Corp. 1990, 2009, Copyright MPI für Festkörperforshung Stuttgart, 1997–2001.
[64] Y.-M. Legrand, A. van der Lee, N. Masquelez, P. Rabu, M. Barboiu, *Inorg. Chem.* **2007**, *46*, 9083–9089.
[65] W. Humphrey, A. Dalke, K. Schulten, *J. Mol. Graphics* **1996**, *14*, 33–38.
[66] *Kappa CCD* Operation Manual, Nonius, Delft, The Netherlands, **1997**.
[67] G. M. Sheldrick, University of Göttingen, Germany, **1997**.
[68] R. Welter, *Acta Crystallogr., Sect. A* **2006**, *62*, s252.
[69] J. F. Larrow, E. N. Jacobsen, C. H. Senanayake, J. Liu, I. Shinkai, *Org. Synth.* **2004**, *Coll. Vol, 10*, 96.
[70] F. Gasbøl, P. Steenbøl, B. S. Sørensen, *Acta Chem. Scand.* **1972**, *26*, 3605.

Received: April 30, 2010
Published Online: July 27, 2010

